Antitumor efficacy and local distribution of doxorubicin via intratumoral delivery from polymer millirods

Brent D. Weinberg,[1] Hua Ai,[2] Elvin Blanco,[3] James M. Anderson,[4] Jinming Gao[3]
[1]*Department of Biomedical Engineering, Case Western Reserve University, Cleveland, Ohio 44106*
[2]*National Engineering Research Center for Biomaterials, Sichuan University, Chengdu, China*
[3]*Simmons Comprehensive Cancer Center, University of Texas Southwestern Medical Center, Dallas, Texas 75390*
[4]*Institute of Pathology, Case Western Reserve University, Cleveland, Ohio 44106*

Received 22 March 2006; revised 13 April 2006; accepted 28 April 2006
Published online 21 November 2006 in Wiley InterScience (www.interscience.wiley.com). DOI: 10.1002/jbm.a.30914

Abstract: The purpose of this study was to evaluate the antitumor efficacy and local drug distribution from doxorubicin-containing poly(D,L-lactide-*co*-glycolide) (PLGA) implants for intratumoral treatment of liver cancer in a rabbit model. Cylindrical polymer millirods (length 8 mm, diameter 1.5 mm) were produced using 65% PLGA, 21.5% NaCl, and 13.5% doxorubicin. These implants were placed in the center of VX2 liver tumors ($n = 16$, ~8 mm in diameter) in rabbits. Tumors were removed 4 and 8 days after millirod implantation, and antitumor efficacy was assessed using tumor size measurements, tumor histology, and fluorescent measurement of drug distribution. The treated tumors were smaller than the untreated controls on both day 4 (0.17 ± 0.06 vs. 0.31 ± 0.08 cm^2, $p = 0.048$) and day 8 (0.14 ± 0.04 vs. 1.8 ± 0.8 cm^2, $p = 0.025$). Drug distribution profiles demonstrated high doxorubicin concentrations (>1000 μg/g) at the tumor core at both time points and drug penetration distances of 2.8 and 1.3 mm on day 4 and 8, respectively. Histological examination confirmed necrosis throughout the tumor tissue. Biodegradable polymer millirods successfully treated the primary tumor mass by providing high doxorubicin concentrations to the tumor tissue over an eight day period. © 2006 Wiley Periodicals, Inc. J Biomed Mater Res 81A: 161–170, 2007

Key words: biodegradable polymer; polymer implants; intratumoral drug delivery; VX2 tumor; minimally invasive therapy

INTRODUCTION

Minimally invasive, intratumoral strategies for the treatment of solid tumors promise to substantially improve the therapeutic outcomes for many cancers. Systemic chemotherapy is often limited by severe toxicity and patient morbidity,[1,2] and local cancer therapy can overcome this limitation by maximizing drug delivery to malignant tissues while minimizing systemic exposure to chemotherapeutic drugs.[3] Recent progress in imaging technology has created an unprecedented opportunity for minimally invasive treatment of solid tumors.[4] With image guidance, radiologists can pinpoint the spatial location of solid tumors and use percutaneous procedures to administer local treatments.[5–7] Combining minimally-invasive treatment with controlled release technology provides opportunities for treating cancers in a safe and effective manner by placing drug-loaded implants directly into solid tumors.[8] However, many studies are still needed to understand the local distribution of drugs released from intratumoral implants as well as their efficacy in treating the desired volume of tumor.

Several strategies for local chemotherapy of tumors have been developed as reviewed recently by Goldberg et al.[9] Regionally administered chemotherapy schemes, such as intrahepatic artery infusion for liver cancer[3] or intrapleural infusion for lung cancer,[10,11] have improved clinical patient outcomes by changing drug pharmacokinetics to provide increased drug concentrations to tumor tissues while minimizing toxicity associated with treatments. To further increase the specificity of chemotherapy, other studies have implemented direct injections of anticancer agents into tumors.[12,13] Irregular distribution of the drug and rapid clearance from the tumor site results in treatments that are highly dependent on the timing and frequency of the drug injections, which must be chosen to maximize tumor exposure to drug. These studies point to the utility of a controlled release device,

Correspondence to: J. Gao; e-mail: jinming.gao@utsouthwestern.edu

Contract grant sponsor: NIH; contract grant numbers: R01 CA090696, T32 GM07250, R01 CA090696

which can ensure the drug is properly localized and can release drug in a desired amount of time, maximizing the effect of drug on the tumor tissue.[14]

Drug-containing devices such as polymer implants,[15,16] hydrogels,[17,18] and injectable microparticles[19,20] provide additional options for controlling drug release to tumors. Polyanhydride wafers have been studied extensively for the delivery of anticancer agents and are clinically approved (Gliadel®) for the delivery of BCNU to malignant gliomas.[21] Multiple formulations of drug-containing microspheres have been shown to have antitumor effects both in animal studies and preliminary clinical trials.[14,22] Despite these successes, drug distribution from these devices is often limited to only a few millimeters away from the device.[23,24] Moreover, these implant strategies have only been attempted in a small subset of tumor types, and further studies are necessary to understand their drug release and its effects on treated tumor cells.

With the goal of developing a minimally invasive treatment strategy for liver cancer, we have designed doxorubicin-containing, biodegradable polymer implants for intratumoral drug delivery. These polymer implants were designed as cylindrical rods, or millirods (diameter 1.6 mm, length 8.0 mm), composed of poly(D,L-lactide-*co*-glycolide) (PLGA), which can be administered with image-guidance through the bore of a 14-gauge biopsy needle. Previous studies have established the release properties of these implants in both normal and radiofrequency (RF) ablated liver tissues,[25–27] modeled the transport of drug through these tissues,[28] and established techniques for customizing the release rate of these millirods.[29,30] However, the drug distribution from and efficacy of these implants in tumor tissue, which is considerably different from normal tissue in vascularity and transport properties,[31] is currently unknown. In this study, we chose doxorubicin as the therapeutic agent because of its wide use in the treatment of primary and metastatic liver cancers.[32,33] In addition, its natural fluorescence permits quantitative measurement of drug concentration in tissue slices from the tumor.

While other studies have established the initial proof of concept for minimally invasive, intratumoral chemotherapy,[34] few studies of intratumoral therapies have simultaneously measured local drug concentration and tumor histology to correlate tumor response to drug exposure. Targeting this goal, we selected an aggressive, realistic model of hepatic cancer (rabbit VX2 tumor) that has been widely used in studies of minimally invasive tumor treatments.[35,36] A rapid delivery implant was chosen to provide the highest possible drug concentrations early in the study to maximize the initial tumor kill from the treatment and minimize the amount of time in which tumor cells might become doxorubicin resistant. Treatment effects were gauged by monitoring tumor size through gross tissue measurements, drug distribution through fluorescent imaging of tissue slices, and cell morphology through histology. Using adjacent tumor sections for histology and fluorescent drug measurement allowed for direct correlation of drug concentrations with drug effects. Results from this study provide considerable insights for the future development of intratumoral implants as part of clinical cancer therapy.

MATERIALS AND METHODS

Materials

Poly(D,L-lactide-*co*-glycolide) (PLGA; 1:1 lactide/glycolide; inherent viscosity 0.65 dL/g) was obtained from Birmingham Polymers (Birmingham, AL). Tris-buffered saline (TBS, pH 7.4), hydrochloric acid, sodium hydroxide, acetonitrile, and dimethyl sulfoxide (DMSO) were purchased from Fisher Scientific (Pittsburg, PA). Ammonium formate, methylene chloride, poly(vinyl alcohol) (PVA, MW 13,000–23,000 Da, 87–89% hydrolyzed), and Hank's balanced salt solution (HBSS) were acquired from Sigma-Aldrich (St. Louis, MO). Doxorubicin HCl (DOX) (2 mg/mL) in saline (9 mg/mL) was acquired from Bedford Laboratories (Bedford, OH). Teflon tubes (i.d. 1.6 mm) and stainless steel plungers (o.d. 1.6 mm) were purchased from McMaster-Carr Supply Company (Cleveland, OH). Fetal bovine serum was obtained from Cambrex (East Rutherford, NJ).

Implant fabrication

Polymer millirod implants were produced as reported previously[37] and described briefly below. PLGA microspheres (~4 μm in diameter) were produced using a single-emulsion procedure. Doxorubicin/NaCl powder mixture was prepared as follows. The acidic doxorubicin solution (pH 3.0) was basified to pH 9.0 by adding sodium hydroxide, leading to doxorubicin precipitation. The precipitated drug was washed, resuspended, and lowered to pH 3.0 using hydrochloric acid. The resulting concentrated solution was combined with doxorubicin in saline and lyophilized to yield a final powder containing 38.5% doxorubicin and 61.5% NaCl (w/w). To produce the implants, 65% PLGA microspheres and 35% doxorubicin/NaCl powder were mixed with a mortar and pestle, packed into a Teflon tube, and compressed with steel plungers at 90°C for 2 h. The resulting millirods had a composition of 65% PLGA, 21.5% NaCl, and 13.5% doxorubicin (w/w). Control implants were produced using a similar procedure with 100% PLGA microspheres.

Drug release measurement

An *in vitro* release study was performed in TBS (pH 7.4) at 37°C. Millirods ($n = 3$) were placed in vials containing 5 mL of TBS in an incubator/shaker rotating at 100 rpm.

To maintain sink conditions, the implants were moved into a fresh vial of TBS at each sampling point, and the doxorubicin concentration of the solutions was determined by measuring the absorbance at 480 nm (Perkin Elmer Lambda 20 Spectrophotometer) and determining doxorubicin concentration using an extinction coefficient of 17.62 mL/(cm mg). Explanted rods were dissolved in acetonitrile to extract the remaining doxorubicin, and the concentrations of the resulting solutions were measured using HPLC on a C-18 column (150 × 4.6 mm, 5.0 μm particle size) with a mobile phase consisting of 35% acetonitrile and 65% ammonium formate buffer (0.1% w/w) at pH 4.0.

Animals and tumor model

Adult New Zealand White rabbits ($n = 16$; Covance, Princeton, NJ) weighing 2.8–3.2 kg were used. All animal studies were approved by the Institutional Animal Care and Use Committee at Case Western Reserve University and carried out according to its guidelines. For surgical procedures, animals were anesthetized with intramuscular ketamine (40 mg/kg), acetylpromazine (5 mg/kg), and xylazine (5 mg/kg).

The tumor model used in this study was the VX2 carcinoma in rabbit liver. To implant the VX2 cells into the liver, the tumor was first grown for 4 weeks on the hind limb of a donor rabbit. The donor rabbit was euthanized, and the tumor was removed and dissected into small pieces of ~2–3 mm^3. Tumor pieces were stored in fetal bovine serum with 10% DMSO in a liquid nitrogen storage tank. Prior to liver tumor implantation, the tumor pieces were rapidly thawed and washed three times with HBSS.

The implantation surgery was modified from a published procedure[38] and was performed on day −12. The abdomens of the recipient rabbits were shaved and prepped with betadine, after which a midline subxyphoid incision was made. The anterior surface of the middle liver lobe was perforated to a depth of 5 mm with the outer cannula of a 22-gauge angiocatheter, and a piece of tumor measuring ~1 mm^3 was placed into the puncture. Small pieces of cotton and abdominal fat were secured over the puncture site using a single biodegradable suture. This method allows for the growth of a single, well demarcated tumor in the liver of each rabbit. The tumors were then allowed to grow in the liver for 12 days until day 0, when they reached an approximate diameter of 8 mm.

Tumor treatment procedure

For tumor treatment, the rabbits were randomly divided into two groups, a treatment group ($n = 8$) and a control group ($n = 8$), receiving 13.5% and 0% (w/w) doxorubicin implants, respectively. On day 0, the rabbits' abdomens were reopened as described before, and the tumor was located by palpation. The tumor was punctured through the center and perpendicular to the liver surface with an 18-gauge needle. The implant was inserted into the center of the tumor and sutured in place with a piece of cotton and fat on top of the liver. Using sodium pentobarbital euthanasia, half of the animals from each group were then euthanized on day 4, and the remaining half were euthanized on day 8.

Tumor analysis

After tissue removal, tumors were hemisected perpendicular to the implant track and photographed. One half of the tumor was placed in 10% buffered formalin solution and subsequently embedded in paraffin. Alternating slices of paraffin embedded tissue were stained with hematoxylin and eosin (H&E) or left unstained and observed qualitatively with fluorescence microscopy. The other half of the tumor was frozen at −20°C for use in fluorescent imaging analysis. The size of the tumors was evaluated by computing the area of the elliptical cross section through the center of the tumor, which is given by the equation $A = \pi R_l R_s$, where R_l and R_s are the long and short radii of the ellipse, respectively. Statistical comparison was performed using a two-tailed, unpaired t-test with a significance level of 0.05.

Quantitative fluorescence analysis

To determine the amount of drug present in the tissue surrounding the implant, we used a previously established fluorescence imaging technique that takes advantage of doxorubicin's natural fluorescence.[39] Frozen liver sections of 100 μm thick were sliced from each tumor using a cryostat microtome (Microm 505E) and then scanned with a fluorescent imager (Molecular Dynamics Fluorimager SI) using the following conditions: pixel size, 100 μm; bit depth, 16; photomultiplier gain, 850; and sensitivity, high. A calibration between net fluorescence intensity (NFI), the fluorescence minus the liver background fluorescence, and doxorubicin concentration was established by imaging weighed slices of normal liver to which known amounts of doxorubicin were added. This empirical relationship, $NFI = 194[Dox]^{0.67}$, where [Dox] is the doxorubicin concentration in μg/g, was then used to convert fluorescence intensities to doxorubicin concentrations. Mean drug distribution profiles were calculated by averaging 8 profiles evenly spaced by 45° around a fluorescence image. The drug penetration distance was calculated as the average distance between the implant boundary and the point where the drug concentration dropped below 64 μg/g, which is 10 times the therapeutic drug concentration.[40,41] To estimate the total mass of drug remaining in the tumor, we determined the average drug concentration within 4 mm of the implant surface (the approximate size of the original tumor) and multiplied this value by the tissue volume.

RESULTS

Implant properties

The implants used in this study had an average length of 8.0 ± 0.3 mm and an average diameter of 1.49 ± 0.04 mm. *In vitro* the doxorubicin-containing implants were found to release a total of 2.07 ± 0.05 mg of drug over the 8 day period, corresponding to (71.3 ± 1.7)% of the total drug loading. The release half-time was ~4 h, and the vast majority of doxorubicin, 1.98 ± 0.03 mg, was released in the first 24 h.

Tumor size

After tumor removal and sectioning, the VX2 tumors were observed qualitatively and photographed. The tumors were largely spherical, but most of the cross sections were found to be slightly elliptical. Photographs of control and treatment tumors taken on day 8 are shown in Figure 1(A,B), respectively. The control tumor seen in Figure 1(A) is a large and well-circumscribed tumor. The boundary of the tumor is a solid mass of dense tumor tissue, while the center of the tumor is necrotic and consists of a mixture of necrotic cells, inflammatory debris, red blood cells, and edema. Because the center of the tumor was liquid filled, the original location of the implant which was placed in the center of the tumor is not visible in the photograph. The treated tumor seen in Figure 1(B) is also well-circumscribed but considerably smaller than the untreated tumor. The doxorubicin containing millirod was removed from the cavity seen in the center of the tumor, and the remaining tumor is seen as a small, hard shell only a few millimeters in thickness surrounding the implant location.

Tumor measurements taken from the photographs were used to assess the effect of the implant on the growth of the tumor. An example of how the measurements were taken is seen from the white arrows in Figure 1(A). The resulting measurements of cross sectional area were then averaged for all the animals in each group, and the resulting data is shown in Figure 1(C). On day 4, the treatment tumors (0.17 ± 0.06 cm^2) were approximately half the size ($p = 0.048$) of the comparable controls (0.31 ± 0.08 cm^2). The control tumors were also slightly smaller than the 8 mm diameter on day 0, which may be attributed to a response to placement of the drug free implant. By day 8, the size difference was significant, as the treatment tumors (0.14 ± 0.04 cm^2) were more than 10 times smaller ($p = 0.025$) than the controls (1.77 ± 0.78 cm^2). Notable variation in tumor size, especially in the untreated tumors on day 8, is evident, but there is a statistically significant difference in treated and control tumors on both day 4 and day 8.

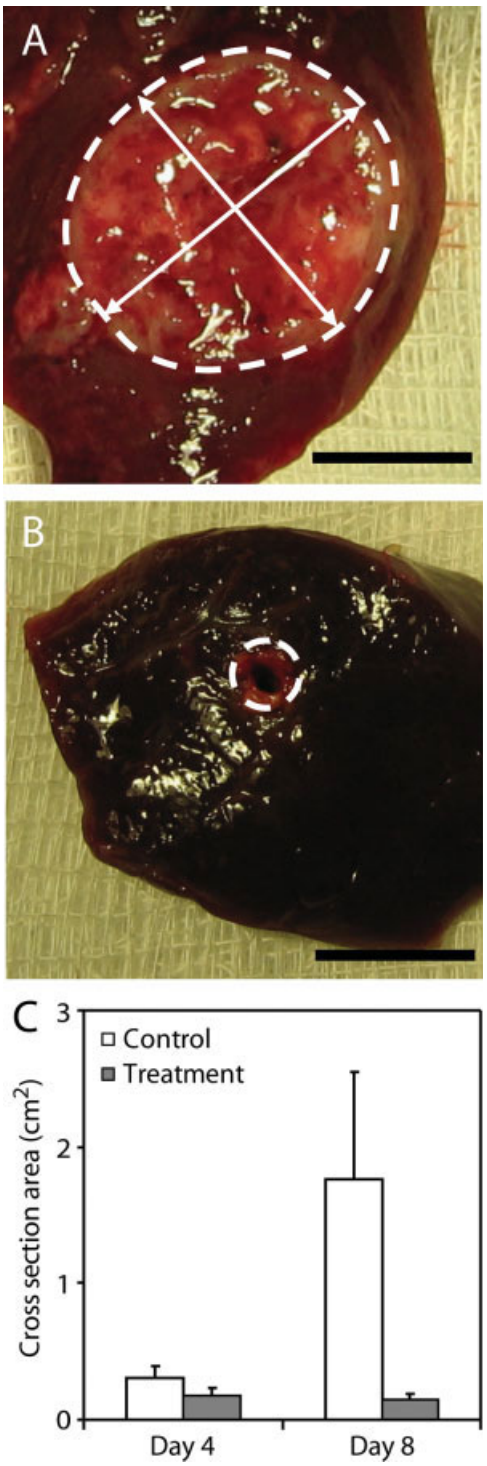

Figure 1. Photographs of a control (A) and a treated (B) tumor cross section on day 8. The boundary between the tumor and normal liver tissue is indicated with a white dotted outline, and the arrows indicate two directions along which the tumor dimensions would be measured to calculate the cross sectional area. The scale bars are 1 cm. Bar graph showing the mean cross sectional area of the treated and control tumors after 4 and 8 days (C). The error bars indicate the standard deviation of each measurement ($n = 4$). [Color figure can be viewed in the online issue, which is available at www.interscience.wiley.com.]

Drug release *in vivo*

A summary of the drug release properties of the implants *in vivo* is shown in Table I. Doxorubicin masses in the original implant, the extracted implant, and in the surrounding tissue as measured by fluorescence are shown along with the values as a percentage of the original doxorubicin loading. For implants extracted on both day 4 and day 8, ~87% of the original drug was released, suggesting that little additional drug was released after day 4. A greater fraction of the drug was released *in vivo* than *in vitro*. Two notable differences are

TABLE I
Summary of Drug Quantities *In Vivo*

	Day 4	Day 8
Original drug loading (μg)	3150 ± 110	3000 ± 190
Drug remaining in extracted implant (μg)	400 ± 40	390 ± 90
Drug released (μg)	2750 ± 130	2610 ± 120
Drug released (%)	87.2 ± 1.5	87.2 ± 2.3
Drug in tissue (μg)	210 ± 120	160 ± 70
Drug in tissue (%)	6.7 ± 3.7	5.5 ± 2.8
Drug penetration distance (mm)*	2.8 ± 0.5	1.3 ± 0.4

Percentages shown are based on the original drug loading. All values are shown ± standard deviation.
*Statistically significant difference between days.

present between the two time points: the tissue at day 4 retains 50 μg more doxorubicin and the doxorubicin penetration distance at day 4 is 1.5 mm further from the implant boundary. Of these differences, however, only the increase in the drug penetration distance is statistically significant ($p = 0.004$). From these measurements, it is also possible to estimate the apparent elimination rate from the tumor tissue by fitting a decaying exponential of the form $D(t) = D_0 \exp(-kt)$ to the known concentrations of drug present in tissue at each time. Using this method, the elimination rate constant from the tumor area was calculated to be $k = 0.42 \pm 0.06$ day^{-1}, which corresponds to an apparent elimination half time from tumor of $t_{1/2} = 1.6 \pm 0.2$ days.

Fluorescent doxorubicin distribution

Local drug distributions from the treated tumors on both day 4 and day 8 were used to evaluate the overall drug exposure to each tumor region. Representative doxorubicin distributions from tumor sections on day 4 and day 8 are shown in Figure 2(A,B), respectively. At both 4 days and 8 days after the millirod implantation, concentrations of drug higher than 1000 μg/g were found in a band surrounding the implant location. These concentrations are considerably higher than the previously reported effective concentration for doxorubicin, 6.4 μg/g.[40,41] Additionally, it can be observed that the band of drug around the implant location appears to be both more intense and thicker in the day 4 distribution as compared to the day 8 distribution. Another characteristic of interest is the large degree of asymmetry in the distributions, which is more pronounced than in previous studies in normal and RF ablated liver tissues.[25] This asymmetry likely reflects the inhomogeneity of the doxorubicin transport properties inside VX2 tumor tissues. Average drug concentration profiles for the distributions in Figure 2(A,B) are shown in Figure 2(C). These profiles quantitatively reaffirm that average concentrations

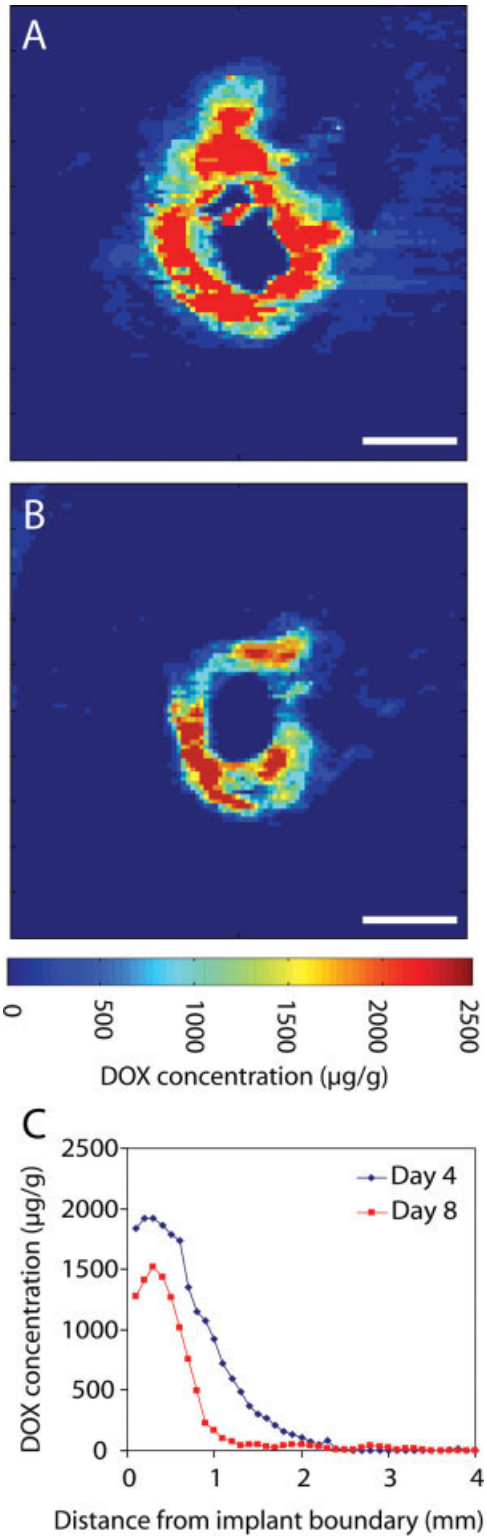

Figure 2. Doxorubicin concentration distribution maps derived from fluorescent imaging of representative tumor sections from the treated group on day 4 (A) and day 8 (B). Before removal, the implant was located in the small clearing found in the center of the image, and the scale bars are 2 mm. From these two distributions, concentration profiles plotting the average doxorubicin concentration against the distance from the implant boundary are shown for both times (C). [Color figure can be viewed in the online issue, which is available at www.interscience.wiley.com.]

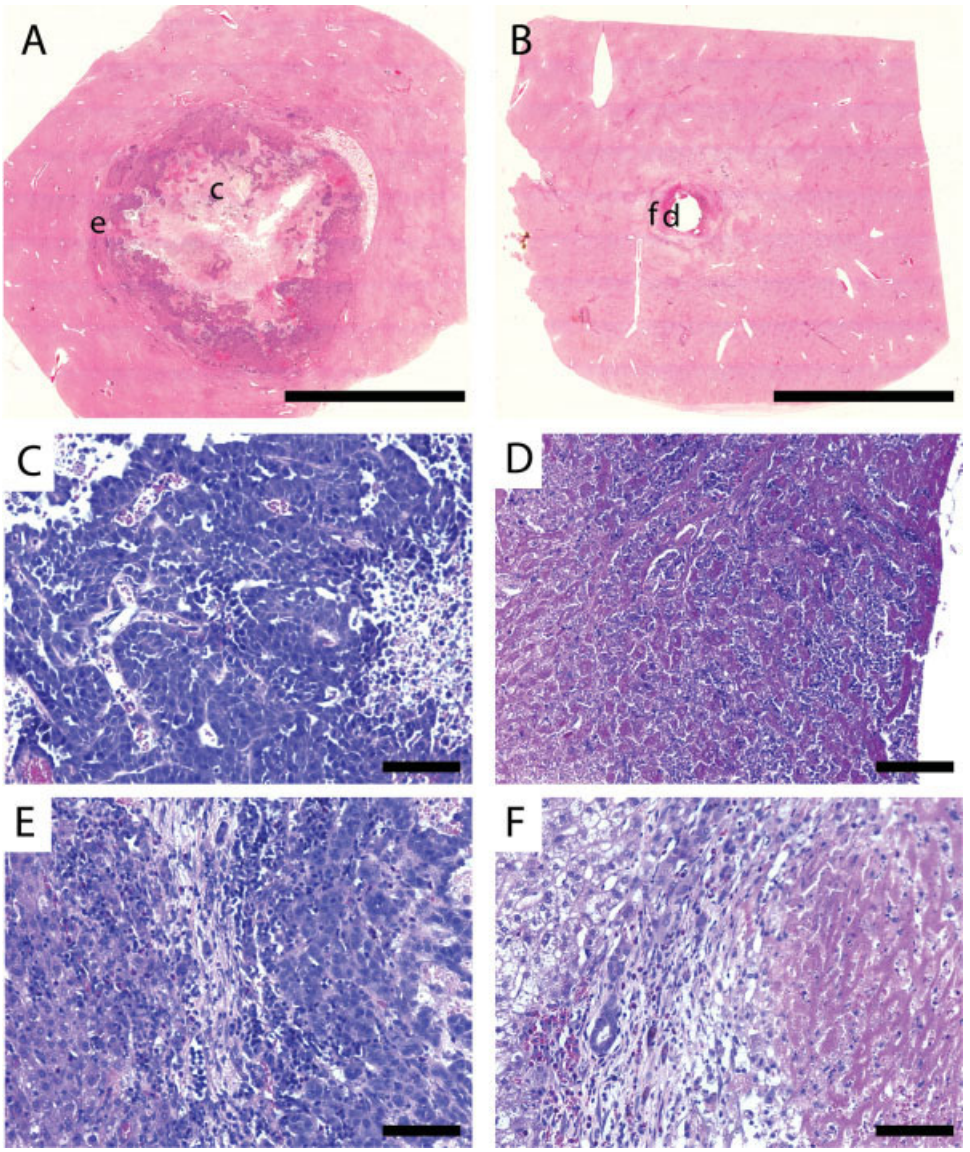

Figure 3. H&E stained sections of control (A, C, E) and treated (B, D, F) tumor sections on day 8. Low magnification images of the control (A) and treated (B) tumors indicate with lower case letters the regions from which the high magnification images are taken. The scale bars are 1 cm. High magnification images of the tumor core for control (C) and treated (D) tumors as well as the tumor/normal liver interface for control (E) and treated (F) tumors are also shown. The clearing on the right side of slide (D) is the original implant location. In (E) and (F), normal liver is found to the left of the panel while tumor is found to the right. All high magnification images (C–F) have scale bars of 100 μm. [Color figure can be viewed in the online issue, which is available at www.interscience.wiley.com.]

near the implant are higher and the drug penetrates to a greater distance in the day 4 distribution. The average doxorubicin concentration within 0.5 mm of the implant boundary in these slices is 1870 ± 60 and 1380 ± 110 μg/g for day 4 and day 8, respectively. In contrast, little to no fluorescence was seen in the control tissue (data not shown).

Histological comparison of tumors

Representative H&E sections of a control and treated tumor on day 8 are shown in Figure 3. The control tumor [Fig. 3(A)] is large and has a boundary of darkly staining viable tumor cells surrounding a core comprised of viable tumor cells mixed with necrotic debris, while the treated tumor [Fig. 3(B)] has a smaller boundary of largely necrotic tumor cells. The higher magnification image from the core of the control tumor [Fig. 3(C)] reveals clusters of large, irregularly shaped tumor cells with darkly staining nuclei interspersed with lighter regions of necrosis and cellular debris. In contrast, the treated tumor core [Fig. 3(D)] is heavily necrotic and contains few viable cells. Cells lack discernible boundaries and have no distinct nuclei, and basophilic remains

have aggregated. Similar differences are visible in the high magnification images of the tumor boundaries [Fig. 3(E,F)]. Again, the control tumor is filled with viable tumor cells while the treated tumor is largely necrotic. Both tumors are separated from normal tissue by a lighter staining fibrous region containing a mixture of tumor and inflammatory cells. Histological comparison of the tumors reveals marked differences between the regions exposed to doxorubicin from the implant and the untreated controls.

H&E histology [Fig. 4(A)] and fluorescent microscopy [Fig. 4(B)] from the same tissue area after 8 days allow for explicit localization of the doxorubicin into three main regions of the treated tumor. Region 1, closest to the implant location, contains dense basophilic and eosinophilic necrotic debris accompanied by high doxorubicin concentrations. Region 2 is filled with less dense necrotic debris characterized by a lack of nuclei and has detectable but considerably smaller amounts of fluorescence. Finally, Region 3 contains the fibrous band separating tumor from normal tissue, which is marked by a dotted band of fluorescent cells skirting the outer tumor boundary. Enlargement of this region [Fig. 4(C)] shows an area of enhanced cellular uptake of doxorubicin. Particularly, the nuclear detail visible in the image indicates the presence of drug in cell nuclei, the primary location of action for doxorubicin. These images indicate that even those cells at the tumor/normal tissue interface have significant doxorubicin exposure over the 8 day period of treatment. Fluorescence in this region was not observed in drug-free controls (data not shown).

While the main tumor mass in the treated animals is necrotic and exposed to high drug concentrations, there is histological evidence that residual viable tumor cells still exist on day 8. An H&E stained section shows cords of tumor cells extending ~1–2 mm from the tumor/normal tissue boundary (Fig. 5). These cells appear to be viable and are far enough from the implant location that they are unlikely to be exposed to therapeutic drug concentrations.

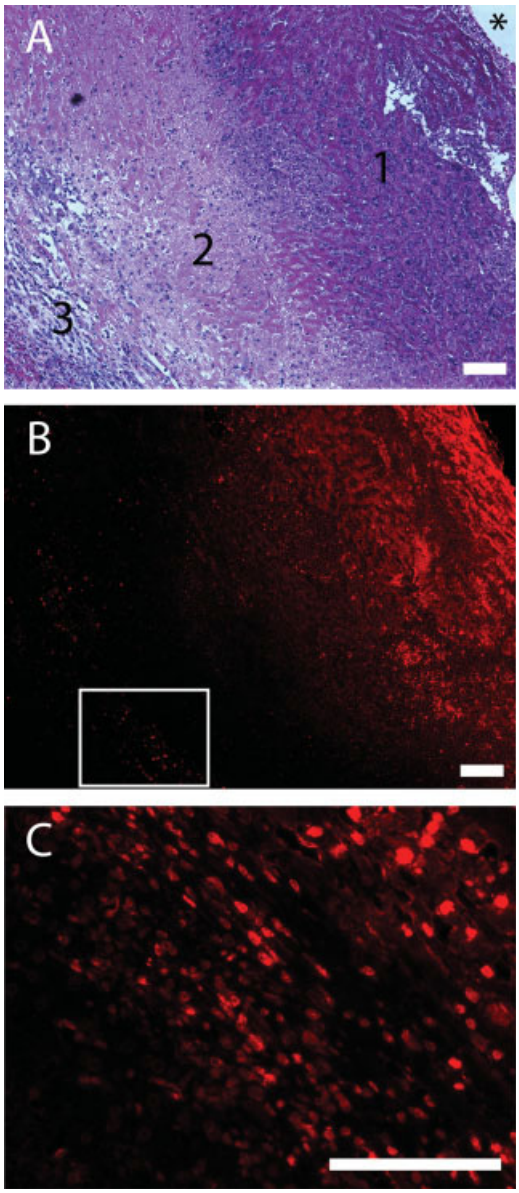

Figure 4. H&E stained and fluorescent micrographs of a treated tumor on day 8. The H&E section (A) illustrates the different tissue regions moving outward from the implant location (*): (1) a dense necrotic region, (2) a sparse necrotic region, and (3) the inflammatory boundary of the tumor. An aligned fluorescence micrograph (B) illustrates the pattern of doxorubicin distribution throughout the tumor regions. A higher magnification image (C) of the area indicated with a white box in (B) shows significant cellular uptake of doxorubicin in the inflammatory boundary of the tumor. All scale bars are 100 μm. [Color figure can be viewed in the online issue, which is available at www.interscience.wiley.com.]

DISCUSSION

In this study, doxorubicin-containing PLGA implants were used to treat VX2 carcinomas in rabbit liver, and the response to treatment was simultaneously evaluated using tumor size, fluorescence drug distribution, and histology. The treated tumors were significantly smaller than the untreated controls at both day 4 and day 8. Histological analysis confirmed the tumor response to drug treatment at cellular level, where regions of viable tumor cells in untreated tumor were replaced by broad regions of necrosis in tumor implanted with doxorubicin millirods. Both macroscopic and microscopic analyses indicate the overall success of the implant for tumor treatment.

A rapidly releasing implant was chosen in this study to maximize drug effect immediately after implantation while still preventing the immediate drug clearance that occurs after direct injection of drug solutions.[14,42] Doxorubicin concentrations greater

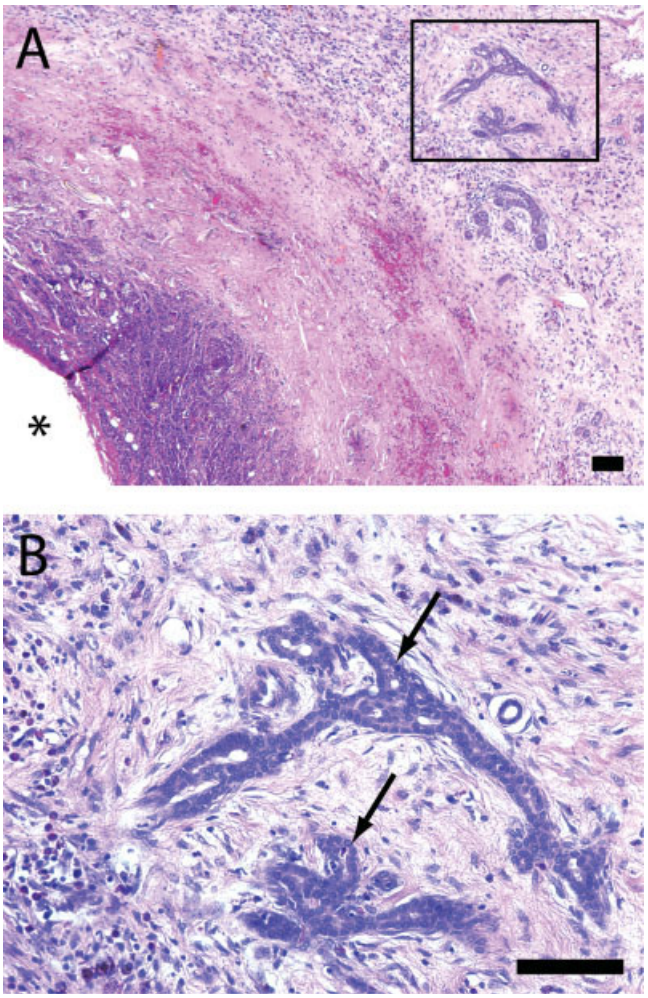

Figure 5. H&E stained micrograph of a treated day 8 tumor showing potential spread of the tumor beyond its circumscribed boundary. A low magnification image (A) indicates the implant location (*) and viable tumor cells (black box), which are magnified in (B). The two arrows indicate cords of viable tumor cells that appear to be spreading beyond the treated zone. The scale bars are 100 μm. [Color figure can be viewed in the online issue, which is available at www.interscience.wiley.com.]

than 100 times the therapeutic level were observed in tumor tissues surrounding the implant even after 8 days. In comparison, intravenously administered doxorubicin is typically eliminated from the plasma with a half-life of ~10 min.[43] Cellular uptake, drug binding to extracellular proteins, and limited perfusion in the necrotic tumor core may each contribute to prolonged drug retention from these intratumoral implants. Qualitatively, the pattern of distributions revealed a greater degree of asymmetry than previously observed in either normal or ablated liver.[28] The irregular drug distribution patterns may be attributed to the inhomogeneity of tumor vasculature[31] and greater drug clearance in highly perfused areas. Overall, the doxorubicin-containing implants provided high drug concentrations for a prolonged exposure time, albeit to only a limited region surrounding the implant.

The most surprising aspect of this study is that necrosis extends to the tumor boundary despite the limited drug penetration distance. While the initial tumors had a radius of ~4 mm, the maximum drug penetration distance was less than 3 mm on both day 4 and day 8. These data would suggest that the tumor periphery would not receive adequate doxorubicin to kill the VX2 cells. To the contrary, microscopic examination of histology slides showed that doxorubicin was present at the tumor boundary and necrotic tumor abutted the surrounding normal liver tissue, demonstrating the treatment of entire tumor volume. Two plausible mechanisms could explain this contradiction. In one scenario, doxorubicin may successfully treat the tumor mass without reaching 4 mm from the implant. Rapid release of high drug concentrations eliminates the VX2 cells closest to the implant, causing the tumor shrinkage observed in the study. The collapse of the tumor core subsequently brings the outer tumor boundary closer to the implant interface. Continued diffusion of drug away from the implant simultaneously moves the front of drug penetration outward, where it eventually meets the inwardly moving tumor boundary by day 4. Alternatively, doxorubicin may reach the therapeutic level at 4 mm but be undetected by this study for various reasons. First, the time points in this study were chosen to maximize the information available from drug distribution, tumor pathology, and histology. Peak drug concentrations likely occur earlier, as soon as 24 h after implantation, when doxorubicin may reach the 4 mm tumor boundary.[28] By day 4, drug penetration distances decrease through clearance and tumor shrinkage as described earlier. Second, doxorubicin may be present at undetectable and yet therapeutic levels beyond the measured penetration distances in this study. While previous studies have established an effective doxorubicin concentration at 6.4 μg/g,[40,41] this number was calculated for a transient exposure to a systemically administered treatment. For a prolonged exposure such as that provided by this implant, the effective drug concentration is expected to be even lower. Future studies that differentiate the above two mechanisms will provide significant insights to fundamentally understand drug transport in tumor tissues and their effects on tumor treatment.

Although this study illustrates considerable promise of polymer millirods for local treatment of VX2 tumors, these implants are not without limitations. Viable tumor cells were observed advancing beyond the main front of the tumor (Fig. 5), potentially by lymphatic spread, which is a known mode of metastasis for the VX2 tumor cells[44] as well as many human tumors.[45–47] Although it cannot be assured that these cells would have developed into a recurrent

tumor, future development of intratumoral treatments should actively focus on successfully delivering drug to a margin of safety beyond the main tumor mass to minimize the risk of recurrence.[48]

On the other hand, combined treatment strategies with these implants offer a number of opportunities for complete tumor eradication. For example, radiofrequency (RF) ablation has been shown to facilitate drug distribution and retention in normal tissues through destruction of the tumor vasculature,[28] which makes it a particularly attractive candidate for use with these implants. In a combined therapy, RF ablation could destroy the vast majority of the tumor volume and surrounding vasculature, allowing greater delivery of doxorubicin to the tumor periphery. Other strategies such as systemically administered targeted nanoparticles[49–51] that have demonstrated effective targeting to the well perfused tumor periphery[52] may also prove synergistic to the millirod therapy. Alternatively, these implants could also be used as a neoadjuvant treatment prior to resection. Tissue conserving surgical removal of the smaller, post-treatment tumor could then be performed, minimizing the risk of local recurrence from residual cancer cells. Irrespective of the combined methods, the described polymer implants provide a versatile platform for minimally invasive, intratumoral chemotherapy, and this study provides detailed insight about drug distribution and antitumor efficacy that can be used in their further development.

CONCLUSIONS

In conclusion, doxorubicin-containing millirods have shown considerable success in treating small but aggressive liver tumors in rabbits. The treated tumors were significantly smaller than the control tumors after both 4 and 8 days, and areas adjacent to the implant contained high concentrations of doxorubicin throughout the study. Although the implants were capable of treating larger tumors than expected, the exact mechanism for this success remains incompletely understood. These promising results will open a variety of opportunities to investigate several combined treatment approaches to achieve complete tumor eradication.

BW is supported by DOD predoctoral fellowship BC043453.

References

1. Nabholtz JM, Reese D, Lindsay MA, Riva A. Evidence for the use of chemotherapy in breast cancer. Int J Clin Oncol 2002; 7:254–264.
2. Leung TW, Johnson PJ. Systemic therapy for hepatocellular carcinoma. Semin Oncol 2001;28:514–520.
3. Aguayo A, Patt YZ. Nonsurgical treatment of hepatocellular carcinoma. Semin Oncol 2001;28:503–513.
4. Apisarnthanarax S, Chao KS. Current imaging paradigms in radiation oncology. Radiat Res 2005;163:1–25.
5. Goldberg SN. Radiofrequency tumor ablation: Principles and techniques. Eur J Ultrasound 2001;13:129–147.
6. Dale PS, Souza JW, Brewer DA. Cryosurgical ablation of unresectable hepatic metastases. J Surg Oncol 1998;68:242–245.
7. Vogl TJ, Mack MG, Muller PK, Straub R, Engelmann K, Eichler K. Interventional MR: Interstitial therapy. Eur Radiol 1999;9: 1479–1487.
8. Guerin C, Olivi A, Weingart JD, Lawson HC, Brem H. Recent advances in brain tumor therapy: Local intracerebral drug delivery by polymers. Invest New Drugs 2004;22:27–37.
9. Goldberg EP, Hadba AR, Almond BA, Marotta JS. Intratumoral cancer chemotherapy and immunotherapy: Opportunities for nonsystemic preoperative drug delivery. J Pharm Pharmacol 2002;54:159–180.
10. Su WC, Lai WW, Chen HH, Hsiue TR, Chen CW, Huang WT, Chen TY, Tsao CJ, Wang NS. Combined intrapleural and intravenous chemotherapy, and pulmonary irradiation, for treatment of patients with lung cancer presenting with malignant pleural effusion. A pilot study. Oncology 2003;64:18–24.
11. Tohda Y, Iwanaga T, Takada M, Yana T, Kawahara M, Negoro S, Okishio K, Kudoh S, Fukuoka M, Furuse K. Intrapleural administration of cisplatin and etoposide to treat malignant pleural effusions in patients with non-small cell lung cancer. Chemotherapy 1999;45:197–204.
12. Duvillard C, Benoit L, Moretto P, Beltramo JL, Brunet-Lecomte P, Correia M, Sergent C, Chauffert B. Epinephrine enhances penetration and anti-cancer activity of local cisplatin on rat sub-cutaneous and peritoneal tumors. Int J Cancer 1999;81:779–784.
13. Duvillard C, Romanet P, Cosmidis A, Beaudouin N, Chauffert B. Phase 2 study of intratumoral cisplatin and epinephrine treatment for locally recurrent head and neck tumors. Ann Otol Rhinol Laryngol 2004;113(3 Part 1):229–233.
14. Emerich DF, Snodgrass P, Lafreniere D, Dean RL, Salzberg H, Marsh J, Perdomo B, Arastu M, Winn SR, Bartus RT. Sustained release chemotherapeutic microspheres provide superior efficacy over systemic therapy and local bolus infusions. Pharm Res 2002;19:1052–1060.
15. Brem H, Piantadosi S, Burger PC, Walker M, Selker R, Vick NA, Black K, Sisti M, Brem S, Mohr G, Muller P, Morawetz R, Schold SC. Placebo-controlled trial of safety and efficacy of intraoperative controlled delivery by biodegradable polymers of chemotherapy for recurrent gliomas. Lancet 1995;345:1008–1012.
16. Li Y, Owusu A, Lehnert S. Treatment of intracranial rat glioma model with implant of radiosensitizer and biomodulator drug combined with external beam radiotherapy. Int J Radiat Oncol Biol Phys 2004;58:519–527.
17. Ruel-Gariepy E, Shive M, Bichara A, Berrada M, Le Garrec D, Chenite A, Leroux JC. A thermosensitive chitosan-based hydrogel for the local delivery of paclitaxel. Eur J Pharm Biopharm 2004;57:53–63.
18. Chen FA, Kuriakose MA, Zhou MX, DeLacure MD, Dunn RL. Biodegradable polymer-mediated intratumoral delivery of cisplatin for treatment of human head and neck squamous cell carcinoma in a chimeric mouse model. Head Neck 2003;25:554–560.
19. Almond BA, Hadba AR, Freeman ST, Cuevas BJ, York AM, Detrisac CJ, Goldberg EP. Efficacy of mitoxantrone-loaded albumin microspheres for intratumoral chemotherapy of breast cancer. J Controlled Release 2003;91:147–155.
20. Menei P, Jadaud E, Faisant N, Boisdron-Celle M, Michalak S, Fournier D, Delhaye M, Benoit JP. Stereotaxic implantation of 5-fluorouracil-releasing microspheres in malignant glioma. Cancer 2004;100:405–410.

21. Brem H, Gabikian P. Biodegradable polymer implants to treat brain tumors. J Controlled Release 2001;74:63–67.
22. Berrada M, Yang Z, Lehnert S. Tumor treatment by sustained intratumoral release of 5-fluorouracil: Effects of drug alone and in combined treatments. Int J Radiat Oncol Biol Phys 2002; 54:1550–1557.
23. Strasser JF, Fung LK, Eller S, Grossman SA, Saltzman WM. Distribution of 1,3-bis(2-chloroethyl)-1-nitrosourea and tracers in the rabbit brain after interstitial delivery by biodegradable polymer implants. J Pharmacol Exp Ther 1995;275:1647–1655.
24. Fleming AB, Saltzman WM. Pharmacokinetics of the carmustine implant. Clin Pharmacokinet 2002;41:403–419.
25. Qian F, Stowe N, Saidel GM, Gao J. Comparison of doxorubicin concentration profiles in radiofrequency-ablated rat livers from sustained- and dual-release PLGA millirods. Pharm Res 2004;21:394–399.
26. Szymanski-Exner A, Gallacher A, Stowe NT, Weinberg B, Haaga JR, Gao J. Local carboplatin delivery and tissue distribution in livers after radiofrequency ablation. J Biomed Mater Res A 2003;67:510–516.
27. Szymanski-Exner A, Stowe NT, Lazebnik RS, Salem K, Wilson DL, Haaga JR, Gao JM. Noninvasive monitoring of local drug release in a rabbit radiofrequency (RF) ablation model using X-ray computed tomography. J Controlled Release 2002;83:415–425.
28. Qian F, Stowe N, Liu EH, Saidel GM, Gao JM. Quantification of in vivo doxorubicin transport from PLGA millirods in thermoablated rat livers. J Controlled Release 2003;91:157–166.
29. Qian F, Saidel GM, Sutton DM, Exner A, Gao JM. Combined modeling and experimental approach for the development of dual-release polymer millirods. J Controlled Release 2002;83: 427–435.
30. Qian F, Nasongkla N, Gao JM. Membrane-encased polymer millirods for sustained release of 5-fluorouracil. J Biomed Mater Res 2002;61:203–211.
31. Jain RK. Delivery of molecular and cellular medicine to solid tumors. Adv Drug Deliv Rev 2001;46:149–168.
32. Clavien PA, Selzner N, Morse M, Selzner M, Paulson E. Downstaging of hepatocellular carcinoma and liver metastases from colorectal cancer by selective intra-arterial chemotherapy. Surgery 2002;131:433–442.
33. Leung TW, Patt YZ, Lau WY, Ho SK, Yu SC, Chan AT, Mok TS, Yeo W, Liew CT, Leung NW, Tang AM, Johnson PJ. Complete pathological remission is possible with systemic combination chemotherapy for inoperable hepatocellular carcinoma. Clin Cancer Res 1999;5:1676–1681.
34. Jackson JK, Gleave ME, Yago V, Beraldi E, Hunter WL, Burt HM. The suppression of human prostate tumor growth in mice by the intratumoral injection of a slow-release polymeric paste formulation of paclitaxel. Cancer Res 2000;60:4146–4151.
35. Ramirez LH, Zhao Z, Rougier P, Bognel C, Dzodic R, Vassal G, Ardouin P, Gouyette A, Munck JN. Pharmacokinetics and antitumor effects of mitoxantrone after intratumoral or intraarterial hepatic administration in rabbits. Cancer Chemother Pharmacol 1996;37:371–376.
36. Yoon CJ, Chung JW, Park JH, Yoon YH, Lee JW, Jeong SY, Chung H. Transcatheter arterial chemoembolization with paclitaxel-lipiodol solution in rabbit VX2 liver tumor. Radiology 2003;229:126–131.
37. Qian F, Szymanski A, Gao JM. Fabrication and characterization of controlled release poly(D,L-lactide-co-glycolide) millirods. J Biomed Mater Res 2001;55:512–522.
38. Geschwind JF, Ko YH, Torbenson MS, Magee C, Pedersen PL. Novel therapy for liver cancer: Direct intraarterial injection of a potent inhibitor of ATP production. Cancer Res 2002;62:3909–3913.
39. Gao JM, Qian F, Szymanski-Exner A, Stowe N, Haaga J. In vivo drug distribution dynamics in thermoablated and normal rabbit livers from biodegradable polymers. J Biomed Mater Res 2002;62:308–314.
40. Ridge JA, Collin C, Bading JR, Hancock C, Conti PS, Daly JM, Raaf JH. Increased adriamycin levels in hepatic implants of rabbit Vx-2 carcinoma from regional infusion. Cancer Res 1988;48: 4584–4587.
41. Swistel AJ, Bading JR, Raaf JH. Intraarterial versus intravenous adriamycin in the rabbit Vx-2 tumor system. Cancer 1984;53: 1397–1404.
42. Buahin KG, Brem H. Interstitial chemotherapy of experimental brain tumors: Comparison of intratumoral injection versus polymeric controlled release. J Neurooncol 1995;26:103–110.
43. Gabizon A, Shmeeda H, Barenholz Y. Pharmacokinetics of pegylated liposomal Doxorubicin: Review of animal and human studies. Clin Pharmacokinet 2003;42:419–436.
44. Dunne AA, Mandic R, Ramaswamy A, Plehn S, Schulz S, Lippert BM, Moll R, Werner JA. Lymphogenic metastatic spread of auricular VX2 carcinoma in New Zealand white rabbits. Anticancer Res 2002;22:3273–3279.
45. Hida J, Yasutomi M, Maruyama T, Fujimoto K, Uchida T, Okuno K. The extent of lymph node dissection for colon carcinoma: The potential impact on laparoscopic surgery. Cancer 1997;80:188–192.
46. Trocha SD, Giuliano AE. Sentinel node in the era of neoadjuvant therapy and locally advanced breast cancer. Surg Oncol 2003;12:271–276.
47. Yuki K, Hirohashi S, Sakamoto M, Kanai T, Shimosato Y. Growth and spread of hepatocellular carcinoma. A review of 240 consecutive autopsy cases. Cancer 1990;66:2174–2179.
48. Pawlik TM, Scoggins CR, Zorzi D, Abdalla EK, Andres A, Eng C, Curley SA, Loyer EM, Muratore A, Mentha G, Capussotti L, Vauthey JN. Effect of surgical margin status on survival and site of recurrence after hepatic resection for colorectal metastases. Ann Surg 2005;241:715–722, discussion 722–724.
49. Straubinger RM, Arnold RD, Zhou R, Mazurchuk R, Slack JE. Antivascular and antitumor activities of liposome-associated drugs. Anticancer Res 2004;24:397–404.
50. Torchilin VP. Targeted polymeric micelles for delivery of poorly soluble drugs. Cell Mol Life Sci 2004;61:2549–2559.
51. Nasongkla N, Shuai X, Ai H, Weinberg BD, Pink J, Boothman DA, Gao J. cRGD-Functionalized polymer micelles for targeted doxorubicin delivery. Angew Chem Int Ed Engl 2004;43:6323–6327.
52. Jain RK. Transport of molecules, particles, and cells in solid tumors. Annu Rev Biomed Eng 1999;1:241–263.